Int. J. Bio-Inorg. Hybd. Nanomat., Vol. 2, No. 3 (2013), 407-422

International Journal of Bio-Inorganic Hybrid Nanomaterials

Photocatalytic Coating Using Titania-Silica Core/Shell Nanoparticles

Hossein Abdollahi[1], Amir Ershad Langroudi[2*], Ali Salimi[3], Azam Rahimi[4], Elham Pournamdari[5]

[1] Ph.D. Student, Color, Resin & Surface Coating (CRSC) Department, Faculty of Polymer Processing, Iran Polymer and Petrochemical Institute (IPPI), 14965/115, Tehran, Iran

[2] Associate Professor, Color, Resin & Surface Coating (CRSC) Department, Faculty of Polymer Processing, Iran Polymer and Petrochemical Institute (IPPI), 14965/115, Tehran, Iran

[3] Assistant Professor, Color, Resin & Surface Coating (CRSC) Department, Faculty of Polymer Processing, Iran Polymer and Petrochemical Institute (IPPI), 14965/115, Tehran, Iran

[4] Professor, Polymer Science Department, Faculty of Science, Iran Polymer and Petrochemical Institute (IPPI), 14965/115, Tehran, Iran

[5] Assistant Professor, Department of Chemistry, Islamshahr Branch, Islamic Azad University, Islamshahr, Iran

Received: 30 April 2013 ; Accepted: 13 July 2013

ABSTRACT

The photocatalytic coatings were prepared via incorporating the modified titania nanoparticles into epoxy-based inorganic-organic hybrid coatings. Titania nanoparticles were first synthesized from tetra-n-butyl titanate using sol-gel methods by two different calcination treatments, i.e., in mild condition (80°C) and 500°C. The formed anatase nanoparticles were further modified as Titania-Silica (TS) core/shell structure. Characterization of the samples was carried by X-ray diffraction (XRD) analysis, Scanning Electron Microscopy (SEM), Transmission Electron Microscopy (TEM), Fourier transform infrared spectroscopy (FT-IR), Energy-Dispersive X-ray (EDX) spectroscopy and UV-Vis spectroscopy. The decomposition of methylene blue (MB) exhibited high photocatalytic activity for the titania nanoparticles embedded with silica phase in core/shell structure. In a comparative study using a commercial P25 titania from Evonik, the synthesized titania samples showed lower size nanoparticles and more uniform distribution of nanoparticles into hybrid binder. However, the degree of anatase crystalline was lower which results to lower photocatalytic activity.

Keyword: Photocatalytic; Hybrid coatings; Titania; Core/shell nanoparticles; Sol-gel process.

(*) Corresponding Author - e-mail: A.Ershad@ippi.ac.ir

1. INTRODUCTION

Recently, the titanium dioxide (TiO_2) or titania organic based films have been intensively investigated for their biological and chemical stability, special optical properties, non-toxicity and low cost [1, 2]. In particular, great attention has been devoted to the study of the photocatalytic properties of titania powders and thin films useful for the removal of pollutants from air or water as self-cleaning surfaces, environmental purification, anti-algal and anti-bacterial coatings [3]. This activity can be obtained due to its ability to mineralize a wide range of organic contaminants and environmental toxins [4]. Under ultraviolet (UV) exposure, the titania nanoparticles can be photo-excited to produce a negative electron in the conduction band and a positive hole in the valence band. In an aqueous environment, the photo-induced electrons and hole pairs react with oxygen or water to generate reactive oxygen species (such as hydroxyl and superoxide radical), which powerfully oxidative and can destroy the structure of various organic molecules [5, 6].

The photocatalytic activity of the titania particles mainly reflects from the physical properties of the titania, such as the crystal structure (amorphous, anatase, rutile, or brookite), the surface area, the particle size, the surface hydroxyls, degree of crystallinity and so on [7, 8]. Different methods have been used to prepare the nanoparticles, such as the chemical precipitation, micro emulsion, hydrothermal crystallization and the sol-gel process [8, 9]. The most common method to form the inorganic core is the hydrolysis of the inorganic alkoxides under mild reaction conditions in the sol-gel process [10]. In the sol-gel processes, titania is usually prepared by hydrolysis and condensation reactions of titanium alkoxides (Ti(OR)n) to form oxide network. Due to high reactivity of titanium alkoxides [11], some chelating reagents, such as Acetyl Acetone (AcAc) and Ethyl Acetoacetate (EAcAc) are often necessary during hydrolysis step. After the condensation step, a calcination treatment (above 400°C) is then required for completing the crystallization [12]. It has been reported that the simple blending of some nano particles such as ZnO, SiO_2 and even the core/shell structure showed enhancement in photocatalytic activity of the titania nanoparticles [13]. The nanoparticles tendency to aggregation in aqueous media and hence reduction of the particles surface area may be diminished by the nanoparticle surface modification [14]. The inorganic-organic hybrids systems combine the advantages of inorganic and organic polymers [15]. The flexibility of the material design, synthesis and properties has gained enhanced research interests in this field [16, 17]. The organo silica-networks may be generated by hydrolysis and condensation reactions of 3-glycidoxypropyl-trimethoxysilane (GPTMS) in water based sol-gel process [18]. The optical properties of the modified GPTMS sols with anatase titania were studied to obtain photo-catalytic active coatings for the development of self-cleaning textiles [7]. It was found that the ability of the GPTMS sol in decomposition of astrazone red corresponds to the GPTMS modification method. The incorporation of silica and Tetraethylorthosilicate (TEOS) has been reported to improve the dispersion of various nanoparticles in a water based environment [19]. One of the most common ways to prepare titania-silica materials is through a sol-gel process where the preparation of titania sol and silica sol is performed separately and then they are mixed to obtain the desired outcome [20]. The method is simple and can be operated at mild condition. The resultant nanoparticles include a core made of the base nanoparticle (titania) and a shell of silica known as a core/shell structure. The silica layer can act as a protector to decrease the effect of the outer environment on the core nanoparticles. Also, the silica surface is electrostatically stable and it improves the dispersion of the core nanoparticles [6]. Although the particle stability and dispersibility can be enhanced after silica coating, some properties of the core component, such as reactivity and thermal stability, also may be altered [21, 22]. Therefore, a mixture of titania-silica is used not

only as a good photocatalyst but also as a support material for chemical catalysts reactions with good dispersion in the water based environments.

A titania-silica core/shell nanostructure, synthesized in sol-gel process, confirmed the synergistic effects of silica on the titania functionality on cotton fabrics [23, 24]. In another study, the water-based colloidal titania-silica core/shell nanoparticles were prepared using aqueous colloidal nano titania and TEOS sol via sol-gel process. The prepared photoactive nanocomposite films from the titania-silica core/shell nanoparticles and poly(MMA-co-MSMA) showed homogenous dispersion of the colloidal titania-silica core/shell nanoparticles and better thermal stability and higher glass transition temperature over pristine binder [25]. A comparative study on the photo degradation of different inorganic, organic and inorganic-organic hybrid binders showed the highest activity of P25 titania from Evonik and tendency to degradation in organic binder [26]. In this research, an inorganic-organic hybrid polymer network was developed as self-cleaning coating. Here, the titania nanoparticles were prepared from tetra-n-butyl titanate at two different calcination treatments. In addition to the photoactivity of the as-prepared nanocomposite coating, detailed characteristics of the coating such as the chemical structure and morphology were investigated and compared with a commercial titania.

2. EXPERIMENTAL

2.1. Materials and Reagents

The Tetraethylorthosilicate (TEOS, ≥98%), tetra-n-butyl titanate (TBT, 97%) from Merck and 3-glycidoxypropyl-trimethoxysilane (GPTMS, 97%) from Alfa Aesar were used as starting materials. Bisphenol A (BPA, 97%, Merck), N-methylimidazol (MI, 99%, Fluka), Acetyl Acetone (AcAc, 99%,

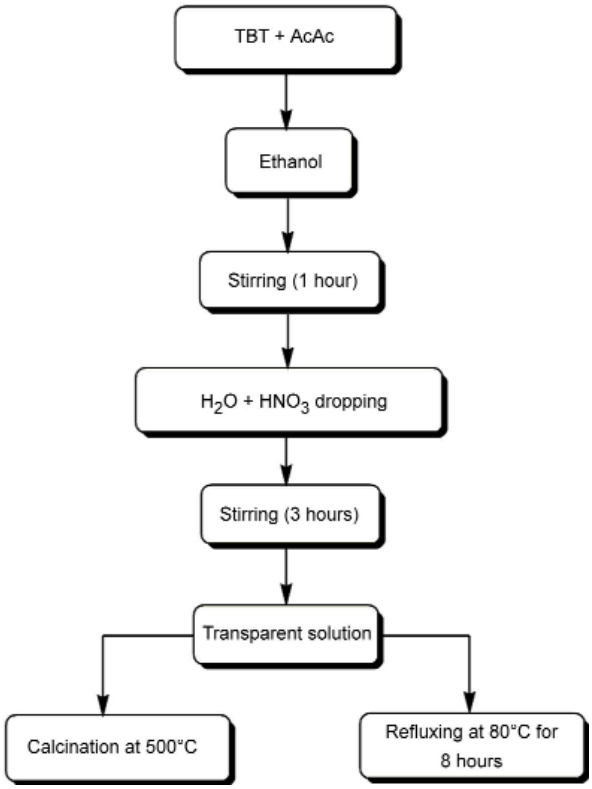

Figure 1: *Diagram of the two methods used in preparation of anatase titania.*

Merck), and Ethanol (99%, Merck) were used as received. The distilled water was used for all experiments. Hydrochloric and nitric acids were purchased from Merck. The titania AEROXIDE® P25 from Evonik was used as a standard reference. The photocatalytic activity of all nanocomposite coatings was investigated using a 40 μM aqueous solution of Methylene Blue (MB, ≥95%, Sigma Aldrich).

2.2. Preparation of sol phase and hybrid coatings

2.2.1. Preparation of titania sol

In sol-gel method, the titania sol phase was prepared from TBT as a precursor in ethanol. The sol phase undergone a hydrolysis/condensation reaction using an acidic water (pH= 2). In order to control the rate of hydrolysis in titanium alkoxides, 0.6 cc of the AcAc was used in 2 cc of TBT. The molar ratios of the reactants were as follows: TBT: HNO_3: Ethanol: AcAc: H_2O = 1:0.018:40:1:100. Then, the mixture was stirred vigorously with a magnetic stirrer at room temperature for 3 h. At next step, two different treatments were employed to obtain the anatase crystal phase. In one method, the prepared sol was refluxed for 8h at 80°C to convert the amorphous titania to anatase crystalline phase (as sample T1). In second method, the prepared sol was heated up to 500°C for 1h in a furnace (as sample T2). Note that the descending rate for annealing temperature was chosen as 10 C/min. The procedure was shown schematically in Figure 1 for the two methods used in preparation of anatase titania.

In the case of using commercial P25 (as sample T3) and sample T2, the particles were dispersed in ethanol at a molar ratio of titania: ethanol = 1:45 using a magnetic stirrer followed by sonication for 10 min on a Bandelin, HD3200, sonicator (KE-76 probe, pulse mode of 0.7 s on and 0.3 s off, 70 W power). Then the sample T2 in powder form and the dried sample T1 (at 60°C over night) were analyzed by XRD technique.

2.2.2. Preparation of titania-silica core/shell nanoparticles

The silica sol was prepared by hydrolysis and condensation of TEOS as a precursor. In this method, 1.3 cc TEOS was first dissolved in 10 cc ethanol and then an acidic water (pH= 2) was added into the solution drop wise. The as-prepared mixture was stirred to precede the hydrolysis reaction at 25°C for 1h. Then, the as-prepared titania sol (sample T1) or titania powders dispersed in ethanol (samples T2 and T3) were added in the silica sol at a molar ratio of (titania:silica 1:1). The resulting mixture underwent two individual hydrolysis/condensation reactions at 25°C for 32 h and at 50°C for 8 h to obtain the titania-silica (TS) core/shell solution. The TS nanoparticles were formed through a strong covalent bonding between OH groups of the titania particles and the OH groups of the silica sol.

2.2.3. Preparation of Epoxy-Silica-Titania hybrid nanocomposite

The series of Epoxy-Silica-Titania (EST) hybrid nanocomposite were prepared by mixing the as-prepared TS core/shell in GPTMS sol followed by stirring vigorously for 25 min at ambient temperature. Wherein, the GPTMS sol was prepared by hydrolysis and condensation of GPTMS in ethanol as solvent, and an acidic water (pH= 2) as a catalyst of hydrolysis-condensation reaction. Then, the BPA as a crosslinker was added to the above solution and stirred vigorously for 4h at ambient temperature. The methyl imidazol as a catalyst (1% wt vs. GPTMS) was used for increasing the cross-linking process. The procedure for the preparation of the EST hybrid nanocomposite was shown in Scheme 1. The molar ratio of reagents in the EST hybrid nanocomposite samples were shown in Table 1.

2.2.4. Film preparation of the nanocomposites samples

The thin films of EST hybrid nanocomposite were fabricated on glass slides (soda lime glass 25.4× 76.2×1.2 mm^3) by a dip coating at ambient conditions. The glass slides were previously cleaned repeatedly in a solution containing 0.1 M HCl and methanol/hexane (40:1) followed by washing with distilled water. Then, the EST thin

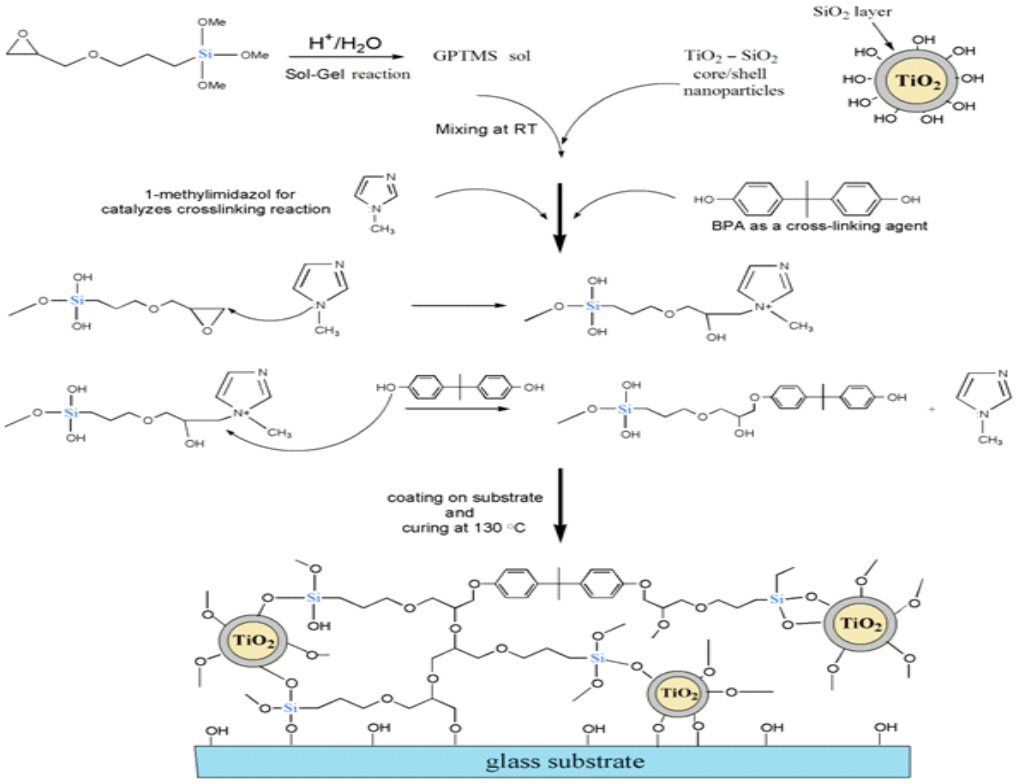

Scheme 1: *Preparation schematic of EST nanocomposite coatings.*

Table 1: *The sol compositions of EST nanocomposites (based on mol fraction).*

Sample	GPTMS	TEOS	TBT	Titania P25	Ethanol	BPA	H_2O
ES	1	0	0	0	5	0.5	3
EST1	1	0.125	0.125	0	0.625	0.5	3.5
EST2	1	0.125	0.125	0	0.625	0.5	3.5
EST3	1	0.125	0	0.125	0.625	0.5	3.5

All mol fraction are based on 1 mol GPTMS.

films were dried at room temperature for 24 h and subsequently were heated in an air-circulating oven at 130°C for about 120 min.

2.3. Instrumentation

The Fourier transform infrared, FT-IR spectra were obtained by using a Bruker (IFS 484, Germany) spectrometer, in the range 400-4000 cm^{-1}. FT-IR spectroscopy was carried out using KBr pellet on a spectrometer, collecting 16 scans at 4 cm^{-1} resolution. The particle size distribution and the average particle size were determined by dynamic light scattering measurements, DLS (SEMA Tech 39 chem du terron 06200, France). Also, the transmission electron microscopy, TEM using a PHILIPS (Model CM120, Netherlands) at an

accelerating voltage 120 kV was used to investigate the average particle size.

The morphological properties of the fractured surface of the EST hybrid nanocomposite were investigated at the by scanning electron microscopy (VEGA\\TESCAN, Czech Republic) at an accelerating voltage of 1500 kV. The distributions of each of the Si and Ti atoms in thin film were investigated by Energy-Dispersive X-ray spectroscopy, EDX mapping (INCA Penta FET×3, Oxford, England).

The titania crystalline phase was investigated by X-ray diffraction measurement, XRD (PW 1800 PHILIPS, Netherlands). The diffraction pattern were obtained using a Cu Kα incident beam (λ= 1.542 Å) at 2θ = 10°-80° and a scanning speed of 4°/min. The voltage and current of X-ray tubes were 40 kV and 30 mA, respectively.

The Brunauer, Emmett and Teller (BET) measurements were carried out to evaluate the specific surface area from nitrogen adsorption-desorption data (CHEMBET-3000 Quantachrom, USA).

The cross-cut adhesion test of the coatings was carried out on 7×5 cm^2 glass substrate using the Scratch-Adhesion Test (Neurtek, Spain). The strength of adhesion of above films coated on glass substrates was measured according to the ASTM D 3359B-02 protocol for adhesion tests (B5 and B0 has best and weak adhesion, respectively).

The ultraviolet-visible (UV-Vis) absorption spectra of the films, deposited on silica glass slides were measured from 200 to 800 nm using a Shimadzu UV-Vis spectrophotometer (UV-3101 PC, Japan). The surfaces of the organic-inorganic hybrid films were cleaned using acetone with a cotton tissue.

The photocatalytic activity of the EST hybrid nanocomposite films coated on glass slide was characterized by inserting coated glass slide into a Petri dish filled with a MB solution. Then, the degradation of MB was evaluated in an aqueous solution (40 μM) under UV illumination at room temperature for 3 h. By measuring the decomposition of MB with the spectrophotometer, the extinctions of the differently treated solutions give information about the photocatalytic activity. The power of the UV lamp was 8 W and the main wavelength of the UV lamp was 254 nm.

Degradation of coating samples was investigated under UV irradiation after 1080h in QUV/Spray chamber (Q-Panel, USA) according to the ASTM D4587 standard. According to the standard procedure, the samples were alternately exposed to

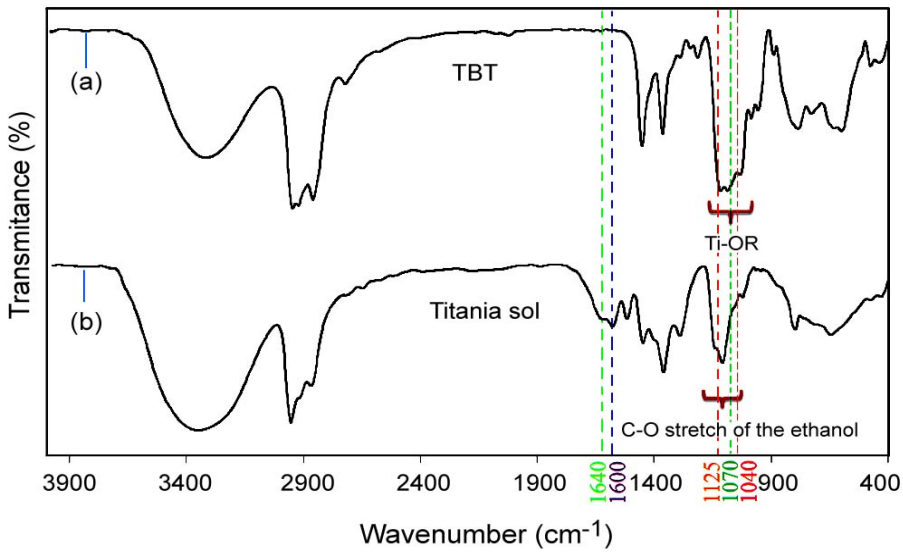

Figure 2: *FT-IR spectrum of the (a) TBT and (b) amorphous titania sol.*

UVA irradiation (340 nm, 0.89 Wm^{-2}) at 60°C for 8 h followed by 4 h of water condensation at 45°C periodically. Effect of accelerated weathering conditions on the degradation of nanocomposite coatings and surface morphology of the epoxy-silica hybrids containing TS nanoparticles was studied using SEM analysis.

3. RESULTS AND DISCUSSION

3.1. FT-IR characterization of titania particles

The FT-IR spectra of the TBT and the titania sol (after hydrolysis reaction) were shown in Figure 2. As shown in Figure 2a, the characteristic absorption peaks for the alkoxy (OR) group of TBT appeared at 1040, 1070 and 1125 cm^{-1} wave numbers [27]. The spectrum of titania sol after hydrolysis reaction indicates for the conversion of titanium tetrabutoxide to titania particles. A broad peak between 3100 and 3600 cm^{-1} in both FT-IR spectra corresponds to the stretching vibration of different O-H groups (free or bonded). The presence of acidic water was confirmed by absorption in the 1600-1640 cm^{-1} region that is assigned to physically adsorbed water (H-O-H bending) [27].

As shown in Figure 2b, there is no absorption peaks related to OR groups. It seems that all four OR groups of TBT were replaced with OH groups of water indicating for a full conversion during the hydrolysis reaction. In fact, the characteristic peaks of OR group were replaced by C-O stretching absorption peaks of the ethanol.

The FT-IR absorption spectrum of the neat titania (AEROXIDE® P25 from Evonik) and the sample TS3 were shown in Figure 3a and b, respectively. As shown in both spectra in Figure 3, the broad and intensive bands with two overlapping components were appeared in the 400-800 cm^{-1} region assigning for the Ti-O and Ti-O-Ti groups [28]. In Figure 3b, the peaks at about 800-810 cm^{-1} and 1080-1105 cm^{-1} correspond to the symmetric vibration of Si-O-Si and asymmetric (Si-O-Si) stretching vibration, respectively [29]. Besides the absorption band at about 950 cm^{-1} corresponds to Ti-O-Si bond in TS nanoparticles [30]. Therefore, the FT-IR spectrum of T3 and TS3 samples indicates for a combination of titania and silica nanoparticles.

3.2. SEM observations of titania particles

The SEM images of the neat titania (sample T3) and sample TS3 nanoparticles were shown in Figure 4.

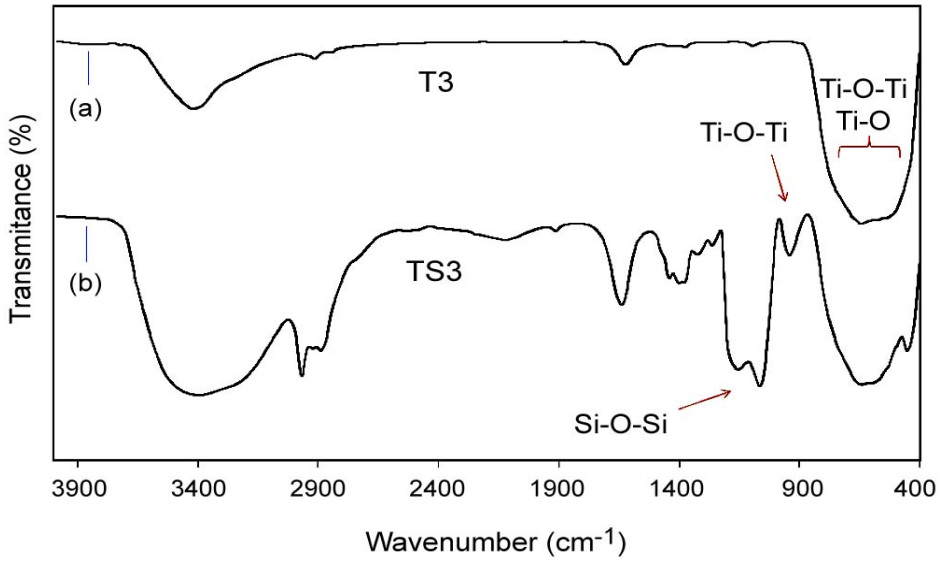

Figure 3: *FT-IR spectrum of the (a) sample T3 and (b) sample TS3.*

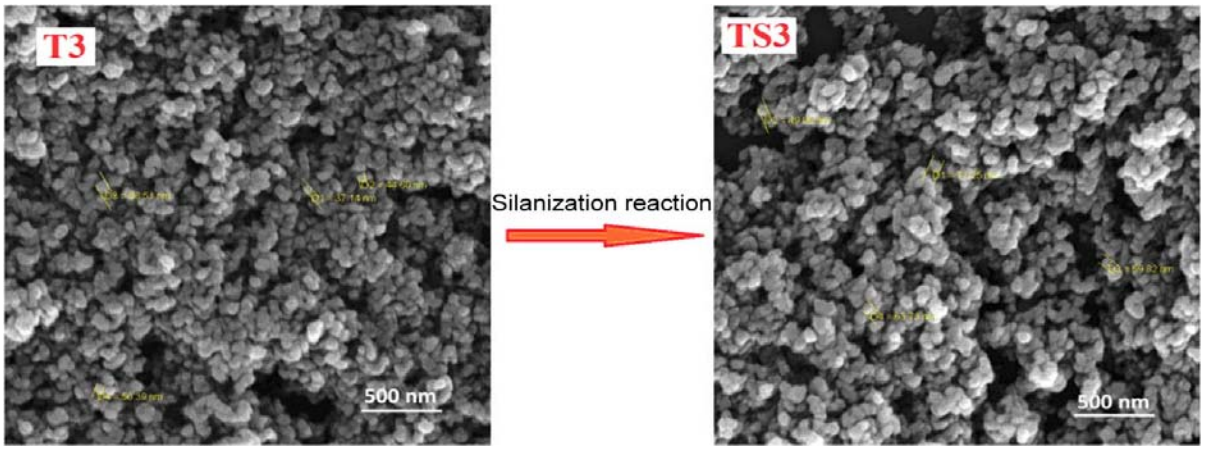

Figure 4: *The SEM images of the neat titania (sample T3) and after silanization (sample TS3).*

The pure titania particles exhibited a somewhat irregular morphology due to the aggregation of primary particles. In comparison with sample T3, the sample TS3 exhibited more porous morphology. The silica surface is electrostatically stable which prevents the aggregation of the titania nanoparticles [6].

3.3. Crystal structure and the specific surface area measurement of titania particles

The XRD patterns of the prepared particles in two individual methods are shown in Figure 5.

As shown in Figure 5a, the diffraction angle at 25.3°, 37.8° and 53.9° correspond to anatase crystal phase for the sample annealed at 500°C (calcinated powder). As shown in Figure 5b, the diffraction angles of the anatase phase (the major peak at 2θ= 25.3°) [31] are evident for the particles formed in sol phase after refluxing. According to the Figure 5, it can be clearly understood that the anatase structure in titania sol phase after refluxing (sample T1) was much less than the calcinated powder (sample T2). Thus, the prepared coatings from these nanoparticles contain the anatase structure. While the coating was prepared from T3, indicated the existence of anatase (70%) and rutile (30%) structures, simultaneously [32].

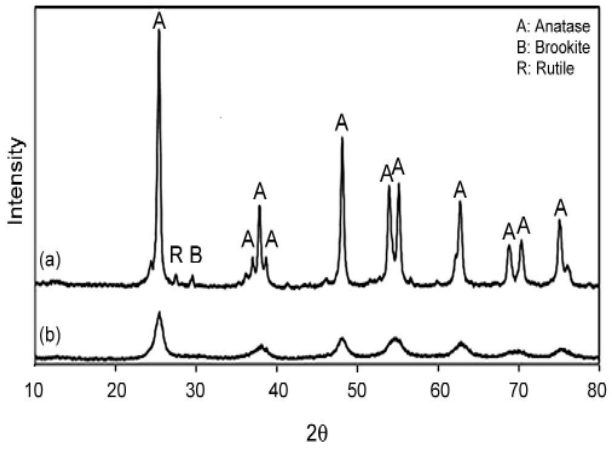

Figure 5: *XRD pattern of the sample (a) T2 and (b) T1. The letters on peaks corresponds for each kind of crystal form in titania.*

The crystallite size of T1 and T2 samples was measured by XRD line profile analysis using the Debye-Scherrer equation (Eq. 1) [33].

$$d = k\lambda / B\cos\theta \qquad \text{(Eq. 1)}$$

Where d is the crystallite size in nm, k a constant (0.9),λ the X-ray wavelength of Cu (1.5406 Å), θ the Bragg's angle in degrees and B is the full width at half maximum of the peak. The results are shown in Table 2. The specific surface area of as-prepared nanoparticles before and after the silanization reaction of titania nanoparticles was measured by

BET test. The BET results were also tabulated in Table 2. According to the BET results for T1 and T2 samples, the decrease in BET surface area from 278.5 m^2/g to 78.3 m^2/g may correspond to an increase in crystal size from 30 nm to 50 nm. Moreover BET results exhibited the amount of specific surface area was considerably increased from 278.5 m^2/g to 325.2 m^2/g for T1 and TS1 samples, respectively, may be due to the formation a shell layer of silica on the titania core. These results are similar to the results of other samples as shown in Table 2. This can be attributed to the fact that surface treatment may provide a porous layer on the surface through grafting. It is believed that grafting on the surface of particles by silanization reaction makes it somehow irregular and rougher and obviously this leads to an increase in the specific surface area [33]. Therefore, silanization reaction increases the specific surface area of nanoparticles, while the crystalline size is constant.

Table 2: *Crystal size and specific surface area for different titania nanoparticles.*

Sample	Crystal size (nm)	crystalline phase	surface area (m^2/g)
T1	30	Anatase	278.5
T2	50	Anatase	78.3
T3	---	Anatase/Rutile	*55.2
TS1	30	Anatase	325.2
TS2	50	Anatase	136.5
TS3	---	Anatase/Rutile	96.3

** BET surface area of P25 (m2/g) 50 ± 15 (product information)*

3.4. Particle size measurements of the titania particles

Dynamic light scattering (DLS) technique was employed to measure size distribution of nano-particles in sample T1 and sample TS1. As shown in Figure 6, the particle size of the titania and TS core/shell were in the range of 5-100 nm (average size of 40 nm) in sample T1 and 9-200 nm (average size of 70 nm) in sample TS1.

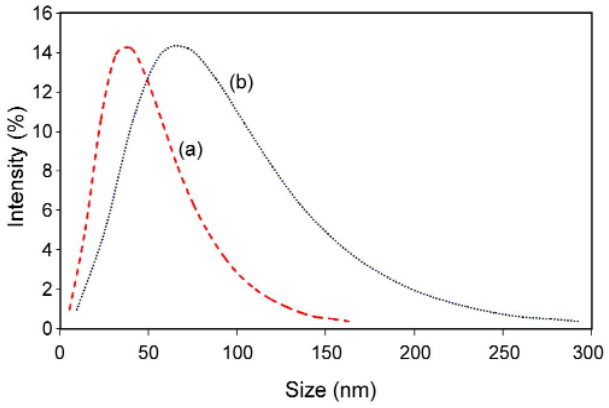

Figure 6: *Particle size distribution of (a) sample T1 and (b) sample TS1 sol.*

3.5. Morphological studies of the hybrid coating

3.5.1. The TEM studies on core/shell structure

The TEM images of the amorphous titania in the sol solution and TS core/shell nanoparticles in EST1 and EST2 nanocomposites were represented in Figure 7a, b and d, respectively. Note that the Figure 7c represents a magnification of core/shell structure of the Figure 7b.

As seen in Figure 7a, titania sol shows irregular shape particles with particle size of about 35 nm. While in Figure 7b and 6c, the titania particles have a regular five-sided shape, which probably reflects the crystalline state of particles and confirmed that anatase crystals formation during refluxing.

Furthermore, Figure 7b shows the formation of silica layer on the titania particles with a thickness of about 15 nm. The TEM images were in good agreement with those of DLS analysis. The difference between the average size of sample T1 and sample TS1 in DLS measurements refers as twice of shell thickness in TEM images, i.e., 15 nm. Figure 7d shows the inorganic particle sizes in EST2 nanocomposites. As seen in Figure 7d, the TS2 nanoparticles had irregular shape particles with average particle size of about 80 nm while, the particle distribution of TS2 in the hybrid coating was not as well as TS1.

3.5.2. The scanning electron microscopy studies on nanoparticles dispersion

After addition of the TS nanoparticles in the

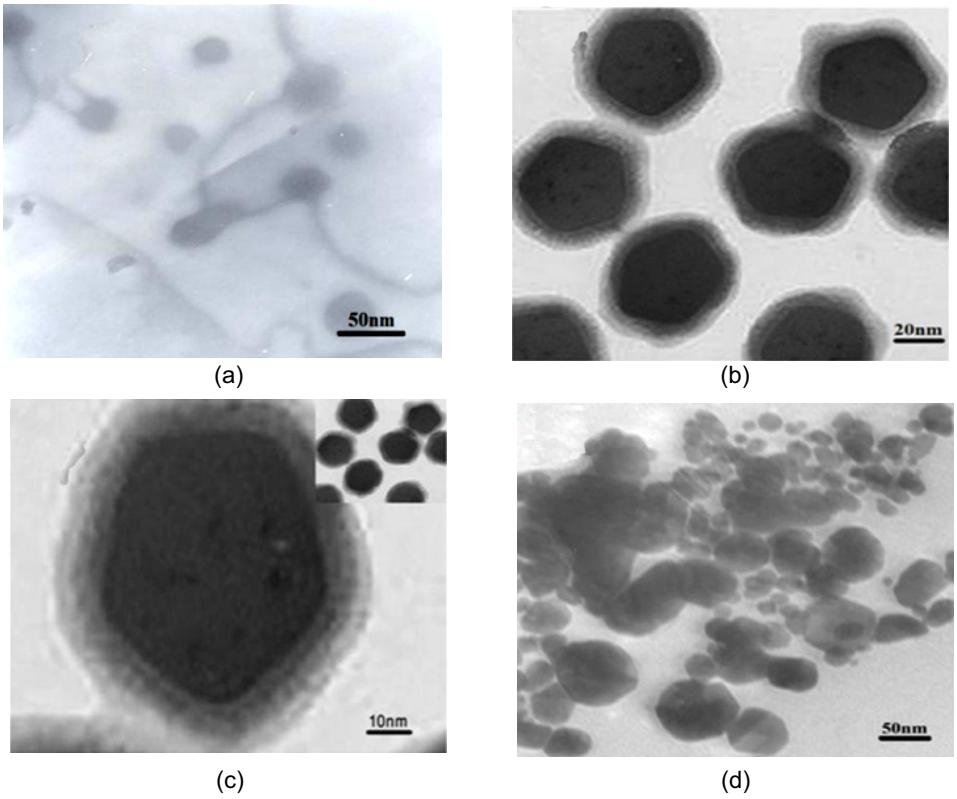

Figure 7: *TEM images of (a) the amorphous titania sol, (b) TS1 core/shell nanoparticles in sample EST1, (c) a magnification of part (b) and (d) TS2 nanoparticles in sample EST2.*

GPTMS sol, these coating solutions were applied onto the glass slides by dip coating method. The map of Si atoms for EST1 was shown in Figure 8a and maps of Ti atoms were shown for EST1, EST2 and EST3 in Figure 8b to d.

It can be seen from the SEM micrographs that distribution of these nanoparticles in the organic-inorganic hybrid coatings was uniform. The uniform distribution of TS core/shell nanoparticles is due to the presence of the silica which prevents agglomeration of titania and inhibits the tendency of titania for phase separation. Since the inorganic parts of polymeric hybrid and particle's shell consists similar atoms and silica surface is electro-statically-stable good distribution of core/shell nanoparticles was resulted in the epoxy-silica hybrid system. Nonetheless, the Ti maps in Figure 8 shows that distribution and dispersion of nano-particles is not similar in all samples.

The sample prepared at mild condition (TS1 sol) shows a better distribution and dispersion than other sample (TS2 and TS3 powders). The distribution and dispersion quality of nanoparticles in EST nanocomposites can influence on the material properties such as optical property which will be discussed in next section [34].

3.5.3. Optical quality of the hybrid coating

The UV-Vis spectra of the as-prepared thin films were shown in Figure 9.

As shown in Figure 9, The ES hybrid thin film demonstrates the prominent peak at ~320 nm attributed to $\pi \rightarrow \pi^*$ transition of the benzene rings of BPA curing agent. The bare titania shows the typical absorption band at 300-400 nm [35]. The photocatalytic activities of titania are directly related to the intensity of UV absorption.

In the visible region (λ>400 nm), the ES film shows good transmission of light. Three phenome-na can be considered for the incident beam as

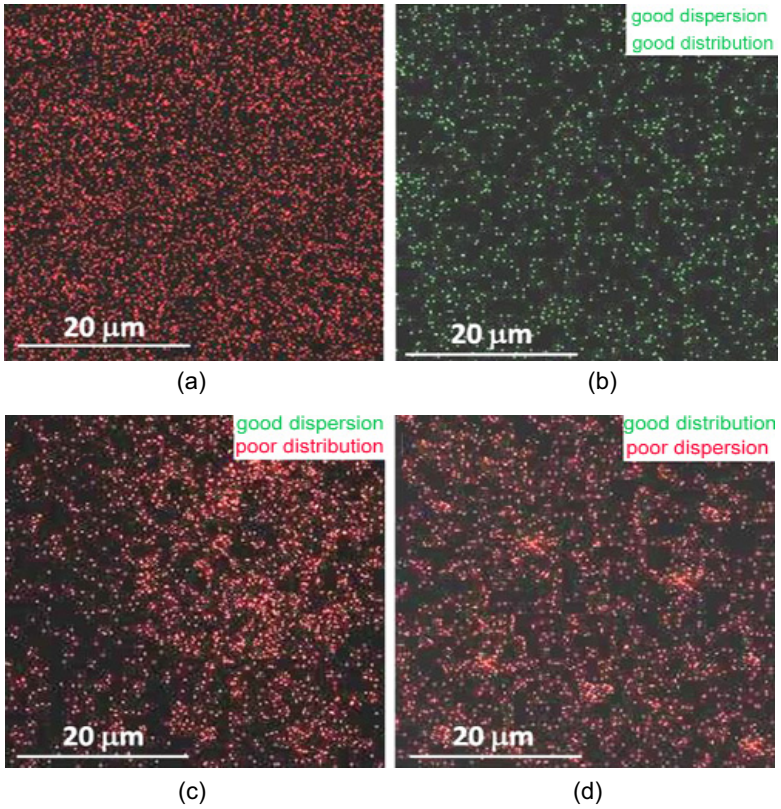

Figure 8: *Inorganic-Organic Hybrid films on glass by sol-gel processing. (a) Si-mapping of EST1, and Ti-mapping of (b) EST1, (c) EST2 and (d) EST3.*

absorption, diffraction and transmission. The sample EST1 was yellowish in color due to complexion of TBT-AcAc. Therefore, in the visible region a higher absorption can be attributed to the color of sample EST1, as seen in Figure 9. While EST2 and EST3 (particularly EST3 due to poor dispersion of TS3 nanoparticles) caused the scattering of light in the visible region. So, the sample EST2 and EST3 were semi-transparent (see Figure 10 c and d) due to the presence of titania nano powder. However, the differences in absorption spectra for the samples EST2 and EST3 can be related to the differences in diffraction of the incident beam. Since these samples have poor distribution (EST2) or poor dispersion (EST3) of TS nanoparticles. These results were also in agreement with Ti mappings and confirmed by transparency measurements of the samples which were presented in Table 3.

Absorption of light below at 300-400 nm is due to the excitation of electrons from the valence band (VB) to the conduction band (CB) of titania. The sample EST1 shows slightly red-shift compared to the EST3 film. A red-shift of the absorption edge indicates a decrease in the band gap of titania when annealing at mild condition. The absorption edges of the EST2 films were significantly blue-shifted compared to the EST3. The shift may be attributed to a "size-quantization effect" [27]. As seen in Figure 9, EST1 and EST2 films show the both differences in intensity and width of the absorption peak. Sample EST2 exhibits the higher absorbance in compared to sample EST1 which can be attributed to high crystallinity and larger particle size of titania in it. The difference in the absorption spectra between EST1 and EST2 films indicates that the particles size and thereby optical quality of titania changes by crystallization temperatures, which was in good agreement with XRD investigation. Therefore, Figure 9 demonstrates that the larg-

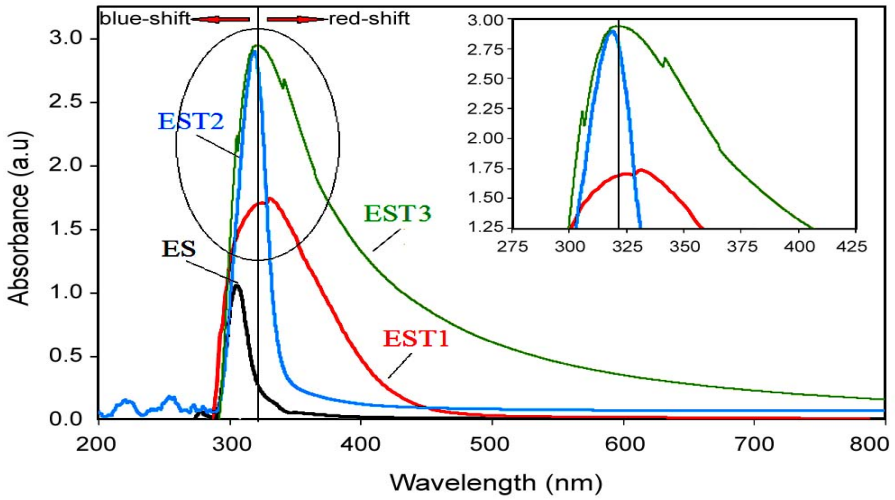

Figure 9: *UV-Vis spectra of the hybrid films.*

er crystals increase the absorption of the light in UV region.

The transparency of the hybrid films were shown in Figure 10. The results were also tabulated in Table3. It was observed that the transparency of ES film was higher than other samples.

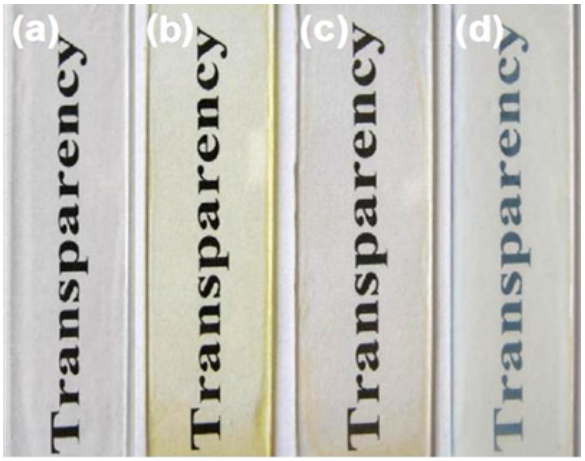

Figure 10: *The pictures of the hybrid films of the (a) ES, (b) EST1, (c) EST2, and (d) EST3.*

3.5.4. Photocatalytic behavior of the hybrid coating

The photocatalytic activities of as-prepared coatings were characterized by the degradation of MB in aqueous solutions which was investigated under an 8 W Xe-UV lamp using a 100 cc reactor. This property of titania depends on its crystallinity, crystalline structure, particle size and surface area of the titania in the coatings [36].

The photocatalytic activity results from the formation of active species that can initiate photo-oxidative degradation of the organic materials by reaction with water or oxygen [37]. The following reaction is photochemical degradation of MB by O_2 in the presence of titania under UV light irradiation (3.2 eV is the band gap energy of the titania), i.e. Figure 11a and b shows the percentage of MB degraded as a function of irradiation time for the as-prepared films.

In Figure 11a, the photocatalyst activity of a thin layer of sample T2 and sample TS2 on glass slide were shown. As seen in Figure 11a, the photocatalyst activity of sample TS2 was more pronounced than sample T2, may be due to the increased specific surface area and the higher concentration of hydroxyl groups on the surface in which transfer electrons more easily. The increase in surface area was observed in BET test results as in Table 2, i.e.,

$$C_{16}H_{18}N_3SCl + 25\ 1/2O_2 \xrightarrow[TiO_2]{h\nu\ (3.2\ eV)} HCl + H_2SO_4 + 3HNO_3 + 16CO_2 + 6H_2O$$

78.3 m2/g for sample T2 to 136.5 m2/g for sample TS2. Another reason is that more negative CB in the presence of silane increases the number of electrons available to titania for initiating decomposition [38].

Table 3: *Transparency measurement of samples.*

sample	Transparency
Uncoated glass slide	92
ES	90
EST1	82
EST2	76
EST3	62.5

Figure 11b shows the MB degradation rate of the coatings on glass slides. It is found that coating prepared from calcinated titania in 500°C (sample EST2) exhibits the highest degree in MB degradation compared with other samples, so that the degradation of MB reached 99% after irradiation for 150 min. It should be pointed out that the particles (T2) in sample EST2 were smaller than particles (T3) in the sample EST3, so the specific surface area is larger as BET results. The specific surface area differs from 78 m^2/g for sample T2 to 55 m2/g for sample T3. Therefore, the average path length of a charge carrier to the surface gets longer and hence emerges a negative effect on the photo activity for sample EST3. As the particle size decreases, the combination of electron-hole decreases and as a result the photocatalytic effect is increases [37]. In addition, the sample EST2 shows higher anatase crystals relative to the sample EST3. Thus, the sample EST2 exhibits higher photo activity relative to sample EST3.

Besides, the sample EST1 shows lower MB degradation than sample ETS2. As mentioned earlier the effective factor on photocatalytic activity is crystallinity and the low photo activity of EST1 is due to its low crystallinity. Simultaneously the higher photocatalytic activity found for particles of sample TS in the sample EST2 compared to sample EST1, which was in good agreement with the XRD results. The XRD test indicated the higher crystallinity for sample T2. However, preparation of the hybrid coatings based on EST1 have some advantages such as simple process without any extensive powder dispersing which can eliminates the probability of agglomeration of titania particles in the coating process and as a result can increase transparency.

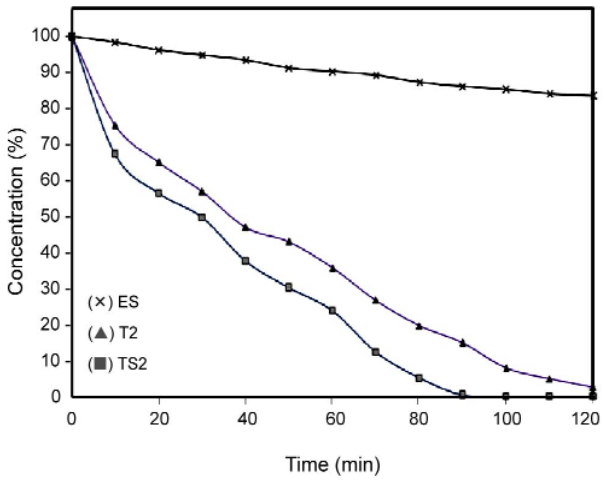

(a)

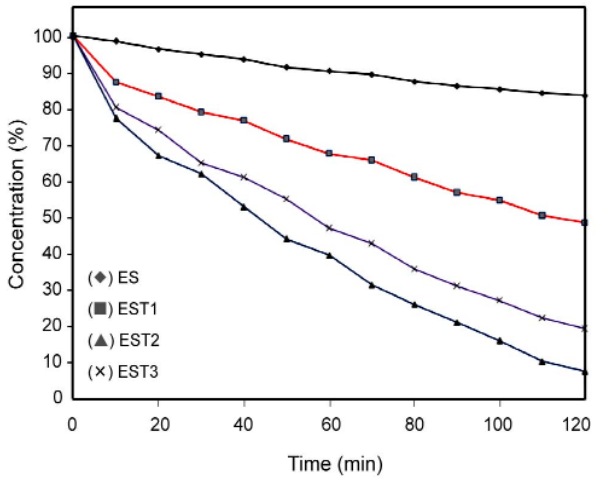

(b)

Figure 11: *Photo degradation of methylene blue.*

3.5.5. Durability of the nanocomposite coatings

SEM micrographs of sample EST1 and sample EST2 after 1080 h exposure to accelerated weathering conditions are shown in Figure 12.

As seen in Figure 12a and b, the coating surface damage was a function of photocatalytic activity of the nanoparticles in the coating. The photo degrada-

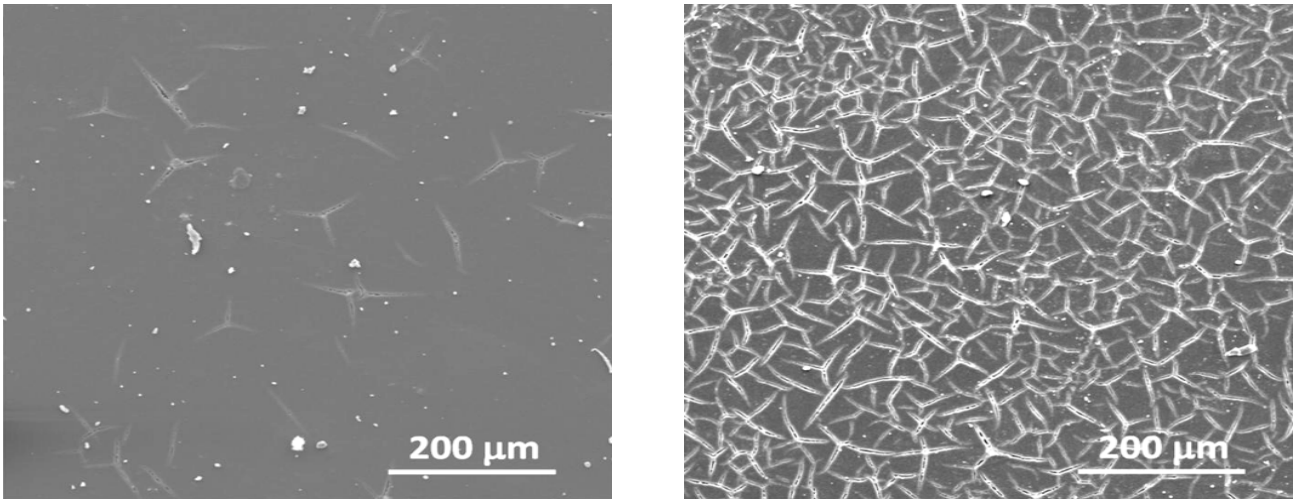

(a) (b)

Figure 12: *Photo degradation of the EST1 (a) and EST2 (b) coatings under 1080h UV irradiation.*

tion was more severe in sample EST2 than sample EST1 which corresponds to higher photocatalytic activity in epoxy hybrid coating containing calcinated titania nanoparticles.

The comparison study on photocatalytic behavior of coating using titania nanoparticles prepared of two different synthesis method showed a challenging decision. In comparison with the sample containing calcinated titania nanoparticles, the use of titania nanoparticle prepared at mild conditions into the epoxy based coating (as sample EST1) resulted to ease of synthesis, lower size nanoparticles, more uniform distribution of nanoparticles into binder, lower anatase crystalline and finally lower photocatalytic activity. However, the photocatalytic behavior of hybrid coating was rather adequate in comparison with the sample EST2. These findings advise the use of titania nanoparticles which were prepared at mild conditions into the epoxy based coating to reach a hybrid coating of rather good photocatalytic behavior.

3.5.6. Coating adhesion measurements

The adhesion of the films on glass surface is based on the condensation of hydroxyl groups of the glass surface and the coating solution. The results were specified as a 5B class (the highest adhesion strength) for the ES and EST1 series and 4B for the EST2 and EST3 series.

Figure 9 shows SEM micrographs of the cross section of coating prepared from Epoxy-Silica hybrid (ES) on the glass slide. The thickness of the films was evaluated to be about ~15 µm. The adhesion test was indirectly supported by the SEM observations on the cross cut section of above film-glass interfaces. In fact, the elongated fibrils were observed in the cross section of coating-glass interfaces showing for high coating adhesion.

Therefore, according to the results of cross-cut test and SEM cross-section, a good level of adhesion was observed between the coatings and the glass substrate. The good coating adhesion may be attributed to the appearance of Si-O-Si covalent bonds at the glass-coating interface [39].

4. CONCLUSIONS

The titania-silica core/shell nanoparticles were successfully prepared from TBT and TEOS via sol-gel method. The crystalline phase of titania sol annealed in low (T1) and high (T2) temperatures were investigated by X-ray diffraction measurement. The results of XRD showed the appearance

of anatase phase in titania nanoparticles. The TEM images exhibited a regular five-sided shape with particle size of about 35 nm forTS1 core/shell nanoparticles, while image of TS2 showed irregular shape particles with particle size of about 80 nm. Furthermore, TEM images showed the formation of silica layer on the titania particles with thickness of about 15 nm. The EDX mapping of Si and Ti showed the sample prepared at mild condition (TS1 sol) has a better nanoparticles distribution and dispersion than other sample (TS2 and TS3 powders) in the organic-inorganic hybrid coatings. For this reason, the transparency of the hybrid coating contain TS1 core/shell nanoparticles was higher than other samples with TS2 and TS3 (i.e., EST2 and EST3). The photocatalytic activity of the prepared titania-silica core/shell nanoparticles as studied by decomposition of MB aqueous solution showed higher photocatalytic behavior. Besides, the decomposition of MB showed the highest photocatalytic activity for EST2 compared to EST1 and EST3 samples mainly due to the lower crystal size and higher surface area of TS2 than TS1 and TS3. In comparison with the coating containing calcinated titania nanoparticles (sample EST2), the use of titania nanoparticle prepared at low temperature into the epoxy based coating (sample EST1) resulted to ease of synthesis (i.e., at mild condition), more uniform distribution of nanoparticles into binder, lower size nanoparticles, lower anatase crystalline and finally lower photocatalytic activity. The Durability of sample EST1 hybrid coating was rather good in comparison with the sample EST2. These findings favor the use of titania nanoparticles prepared at mild conditions into the epoxy based coating to get a hybrid coating of rather good photocatalytic behavior.

REFERENCES

1. Chen D.H., Caruso R.A., *Adv. Funct. Mater*, **23** (2013), 1356.
2. Mihailovic D., Saponjic Z., Radoicic M., Molina R., Radetic T., Jovancic P., Nedeljkovic J., & Radetic M., *Polmy. Adv. Technol.*, **22** (2011), 703.
3. Smitha V.S., Baiju K.V., Perumal P., Ghosh S., & Warrier K.G., *Eur. J. Inorg. Chem.*, **2012** (2012), 226.
4. Allen N.S., Edge M., Sandoval G., Verran J., Stratton J., & Maltby J., *Photochem. Photobiol.* **81** (2005), 279.
5. Moafi H.F., Shojaie A.F., & Zanjanchi M.A., *J. Appl. Polym. Sci*., **127** (2013), 3778.
6. Feng X., Zhang S., & Lou X., *Colloids Surf. B*, **107** (2013), 220.
7. Textor T., Schroter F., & Schollmeyer E., *Macromol. Symp.*, **254** (2007), 196.
8. Gardin S., Signorini R., Pistore A., Giustina G.D., Brusatin G., Guglielmi M., & Bozio R., *J. Phys. Chem. C*, **114** (2010), 7646.
9. Jothibasu S., Kumar A.A., & Alagar M., *High Perform. Polym.*, **23** (1) (2011), 11.
10. Soucek M.D., Johnson A.H., Meemken L.E., & Wegner J.M., *Polym. Adv. Technol*., **16** (2005), 257.
11. Park H.D., Ahn K.Y., Wahab M.A., Jo N.J., Kim I., & Ha C.S., *Macromol. Res.*, **11** (2003), 172.
12. Addamo M., Augugliaro V., Paola A.D., Lopez E.G., Loddo V., Marci G., & Palmisano L., *Thin Solid Films*, **516** (2008), 3802.
13. Ni M., Leung M.K.H., Leung D.Y.C., & Sumathy K., *Ren. Sustain. Energy Rev.*, **11** (2007), 401.
14. Pazokifard S., Mirabedini S.M., Esfandeh M., Mohseni M., & Ranjbar Z., *Surf. Interface. Anal.*, **44** (2012), 41.
15. Nagappan S., Choi M.C., Sung G., Park S.S., Moorthy M.S., Chu S.W., Lee W.K., & Ha C.S., *Macromol. Res.*, **21** (2013), 669.
16. Hamciuc C., Hamciuc E., & Okrasa, L., *Macromol. Res.*, **19** (2011), 250.
17. Yang S.C., Jin J.H., Kwak S.Y., & Bae B.S., *Macromol. Res.*, **19** (2011), 1166.
18. Gharazi S., Ershad-Langroudi A., & Rahimi A., *Scientia Iranica F: Nanotechnol.*, **18** (3) (2011), 785.
19. Mbeh D.A., Franc R., Merhi Y., Zhang X.F., Veres T., Sacher E., & Yahia L., *J. Biomed. Mater. Res. Part. A*, **100A** (2012), 1637.

20. Xu G., Zheng Z., Wu Y., & Feng N., *Ceram. Int.*, **35** (2009), 1.
21. Siddiquey I.A., Furusawa T., Sato M., Bahadur N.M., Alam M.M., & Suzuki N., *Ultrason. Sonochem.*, **19** (2012), 750.
22. Li Q.Y., Chen Y.F., Zeng D.D., Gao W.M., & Wu Z.J., *J. Nanoparticle Res.*, **7** (2005), 295.
23. Qi K., Chen X., Liu Y., Xin J.H., Mak C.L., & Daoud W.A., *J. Mater. Chem.*, **17** (2007), 3504.
24. Pakdel E., & Daoud W.A., *J. Colloid Interface Sci.*, (2013), Article in press.
25. Hwang S.T., Hahn Y.B., Nahm K.S., & Lee Y.S., *Colloids Surf. A*, **259** (2005), 63.
26. Yu D.S., & Ha J.W., *J. Appl. Chem.*, **9** (2005), 93.
27. Zare-Hossein-abadi D., Ershad-Langroudi A., Rahimi A., & Afsar S., *J. Inorg. Organomet. Polym.*, **20** (2010), 250.
28. An Y.C., & Konishi G.I., *Macromol. Res.*, **19** (2011), 1217.
29. Khan S.B., Seo J., Jang E.S., Akhtar K., Kim K.I., & Han H., *Macromol. Res.*, **19** (2011), 876.
30. Park O.K., & Kang Y.S., *Colloids Surf. A: Physicochem. Eng.Asp.*, **257-258** (2005), 261.
31. Halamus T., Wojciechowski P., & Bobowska I., P*olym. Adv. Technol.*, **19** (2008), 807.
32. Bakardjieva S., Subrt J., Stengl V., Dianez M.J., & Sayagues M.J., *Appl. Catal. B*, **58** (2005), 193.
33. Pazokifard S., Esfandeh M., Mirabedini S.M., Mohseni M., & Ranjbar Z., *J. Coat. Technol. Res.*, **10** (2013), 175.
34. Fenouillot F., Cassagnau P., & Majeste J.C., *Polym.*, **50** (2009), 1333.
35. Ameen S., Song M., Kim D.G., Im Y.B., Seo H.K., Kim Y.S., & Shin H.S., *Macromol. Res.*, **20** (2012), 30.
36. Hu Y., & Yuan C., *J. Mater. Sci. Tech.*, **22** (2006), 239.
37. Awitor K.O., Rivaton A., Gardette J.L., Down A.J., & Johnson M.B., *Thin Solid Films*, **516** (2008), 2286.
38. Ni M., Leung M.K.H., Leung D.Y.C., & Sumathy K., *Ren. Sustain. Energy. Rev.*, **11** (2007), 401.
39. Ershad-Langroudi A., Mai C., Vigier G., & Vassoille R., *J. Appl. Polym. Sci.*, **65** (1997), 2387.